Applied Energy 236 (2019) 793–803

Contents lists available at ScienceDirect

Applied Energy

journal homepage: www.elsevier.com/locate/apenergy

# Design of header and coil steam generators for concentrating solar power applications accounting for low-cycle fatigue requirements

Davide Ferruzza*, Martin Ryhl Kærn, Fredrik Haglind

*Department of Mechanical Engineering, Technical University of Denmark, 2800 Kongens Lyngby, Denmark*

## HIGHLIGHTS

- The heating rates of steam generators are limited by thermo-mechanical constraints.
- Traditionally the design of steam generators does not account for low-cycle fatigue.
- The method accounting for low cycle fatigue constraints is presented.
- The results are compared to those obtained without heating rate constraints.
- Heating rates constraints considerably affect the optimal design results.

## ARTICLE INFO

*Keywords:*
Concentrating solar power
Parabolic trough power plants
Steam generator
Heat exchanger design
Heating rates

## ABSTRACT

Concentrating solar power plants are experiencing an increasing share in the renewable energy generation market. Among them, parabolic trough plants are the most commercially mature technology. These plants still experience many challenges, one of which is the cyclic daily start-up and shut-down procedures. These pose new challenges to industrially mature components like the steam generator system, as frequent load changes might decrease their lifetime considerably due to cyclic thermo-mechanical stress loads. In this context, the header and coil design is a promising configuration to minimize the stresses.

This paper presents a method to design the header and coil heat exchangers of the steam generator, taking into account low-cycle fatigue requirements, by defining minimum allowable heating rates for the evaporator and superheater. Optimal designs were obtained by minimizing the total water pressure drops and purchase equipment costs. A comparison with a sizing routine without accounting for low-cycle fatigue constraints was also conducted.

The model was validated against the component data of a 55 MWe power plant, with a maximum deviation on the total area estimation of +2.5%. The results suggest that including the heating rate constraints in the design routine substantially affects the optimal design configuration, with a 41% cost increase for a 1 bar pressure drop. The optimal design for maximizing the lifetime of the components uses tube outer diameters of 38 mm and 50 mm and a low number of tubes per layer (4–10) for the superheater.

## 1. Introduction

Today's growing attention towards renewable energy sources is posing an increasing demand for flexibility towards electricity generation. Concentrating solar power (CSP) plants are experiencing a developing interest in this context. Specifically, the possibility of integrating CSP technology with relatively cheap ways of storing thermal energy allows decoupling the electricity output from the solar input, making these plants suitable for alternating electricity grid loads [1]. Even though an interesting technology, CSP plants are still not fully competitive with respect to fossil-fuel based technologies. From a technical perspective, the fluctuating and stochastic nature of solar radiation causes operating challenges such as frequent variations in load and daily start-up and shut-down procedures. A way to overcome these challenges is to improve the operating performance by maximizing the flexibility of the components given fluctuating loads. By doing so it is possible to utilize solar irradiation as effectively as possible, thereby maximizing the electrical energy production and profitability [2]. On the other hand, in order to preserve the lifetime of certain components, the maximum gradient of temperature (heating

* Corresponding author.
*E-mail address:* daferr@mek.dtu.dk (D. Ferruzza).

https://doi.org/10.1016/j.apenergy.2018.12.030
Received 10 July 2018; Received in revised form 16 November 2018; Accepted 6 December 2018

**Nomenclature**

*Abbreviations*

| | |
|---|---|
| BPVC | boiler pressure vessel code |
| CSP | concentrating solar power |
| D | deaerator |
| ECO | economizer |
| EVA | evaporator |
| HP | high pressure |
| HPI | historical price index |
| HTRI | Heat Transfer Research, Inc. |
| LP | low pressure |
| PTPP | parabolic trough power plant |
| RH | re-heater |
| SGS | steam generator system |
| SH | superheater |
| ST | steam Turbine |
| TEMA | tubular exchangers manufacturers association |

*Subscripts*

| | |
|---|---|
| b | bend |
| dc | downcomer |
| dp | driving pressure |
| e | parallel to the economizer |
| fm | friction and momentum |
| hx | heat exchanger |
| i | inside |
| m | mechanical |
| o | outside |
| r | riser |
| s | parallel to the superheater |
| s | shell |
| T | thermal |
| tl | tube layer |
| txl | tube for each layer |

*Symbols*

| | |
|---|---|
| $\alpha$ | stress concentration factor [–] |
| $\beta$ | thermal expansion coefficient [$K^{-1}$] |
| $\lambda$ | thermal conductivity [W/(mK)] |
| $\nu$ | Poisson ratio [–] |
| $\omega$ | outer to inner diameter ratio [–] |
| $\Phi_w$ | non-dimensional geometrical coefficient [–] |
| $\rho$ | density [$kg/m^3$] |
| $\sigma$ | stress [Pa] |
| $\theta$ | tube coil angle of bend [rad] |
| $f$ | heat exchanger specific cost front head correction factor [–] |
| $f_D$ | Darcy's friction factor [–] |
| $p_{OD}$ | heat exchanger specific cost outer diameter correction factor [–] |
| $r$ | heat exchanger specific cost rear head correction factor [–] |
| $S_l$ | longitudinal pitch [m] |
| $S_t$ | transversal pitch [m] |
| $\nu_T$ | heating rate [K/min] |
| A | area [$m^2$] |
| b | heat exchanger specific cost [USD/$m^2$] |
| c | heat exchanger specific cost correction factor [–] |
| E | Young's modulus [Pa] |
| F | LMTD correction factor [–] |
| h | heat transfer coefficient [W/$m^2$ K] |
| ID | internal diameter [m] |
| L | length [m] |
| OD | outer diameter [m] |
| p | pressure [bar] |
| PEC | purchase equipment cost [USD] |
| S | maximum allowable stress [Pa] |
| T | temperature [°C] |
| t | thickness [m] |
| U | overall heat transfer coefficient [W/$m^2$ K] |
| u | velocity [m/s] |
| y | safety coefficient [–] |

rate) is limited by thermo-mechanical constraints.

Parabolic trough power plants (PTPP) represent the most technically and economically mature technology among CSP plants. They account for around 80% of both the currently installed and planned to be constructed power plants [3–5]. In such power plants, the conventional fossil-fuel fired boiler is replaced by a series of parabolic mirror lenses to concentrate direct beam solar radiation onto the receiver tubes to produce useful high temperature heat. This can be used to produce electricity by a Rankine cycle. The main link between the solar field and the power block is the steam generator system (SGS). It consists of a train of heat exchangers which transfer the useful high temperature heat from a heat transfer fluid (HTF) to the water coming from the condensing line of the Rankine cycle. The temperature of the liquid water is raised until it reaches superheated steam conditions at the inlet of the turbine [4].

Generally the SGS, together with the steam turbines, poses limitations with regards to the rate of the power block start-up [6]. High temperature gradients induce high thermal stresses and therefore limit the lifetime of such components. Specifically the maximum heating rates at which the SGS can experience a temperature increase is limited by the thermo-mechanical stresses on the thick-walled components and junctions, such as, the steam drum, superheater headers and T or Y junctions in the steam pipelines [7–9]. The main limiting component is usually the evaporator steam drum, which is designed as a high pressure vessel with a large diameter, hence consisting of thick walls. Regarding the most conventional single phase heat exchangers, the heating rates are limited by the stresses in the thick tube plates [10]. The maximum heating rates are calculated based on low-cycle fatigue (LCF) theories, by minimizing the resulting stress from a cyclic load and keeping it below a safety threshold to guarantee the required lifetime [11]. It is of common practice in the industry to do so by using the European norm EN 12952-3, which illustrates all the steps to calculate minimum and maximum allowable heating rates [12].

Many CSP plants currently in operation, have SGSs which were designed as conventional heat exchangers, not optimized for transient operation [13]. One of the possible configurations that can be used to overcome such problems is the header and coil design. In contrast to what happens in kettle reboiler type evaporators or TEMA (Tubular exchangers manufacturers association) heat exchangers, the coil type heat exchanger does not have thick tube plates. The heat transfer fluid (HTF) flows are distributed to the tube bank via a circular manifold (header). The round shape of the header results in lower thickness requirements for pressure resistance, and therefore, there are low thermal stresses which are proportional to the square of the thickness [14]. A similar reasoning can be applied to the single phase heat exchangers, such as the economizer (ECO), re-heaters (RH) and superheaters (SH). Also in this case the typical TEMA F or H heat exchangers are characterized by thick tube plates which reduce their transient response.

There is an increasing interest for the design and analysis of steam generator systems. For instance, Mercati et al. [15] developed a method to design a SGS for a system which aimed at producing both superheated steam and hydrogen. The authors also evaluated the impact of

the steam generator performance on the energy conversion system behavior. Many of the previous works on steam generator investigations are related to nuclear applications. For instance, Liu et al. [16] and Chen et al. [17] investigated a natural circulation SGS for pressurized water reactors by means of optimization algorithms. Recently, due the increasing interest for renewable energy sources, there has been an increasing focus on the design of steam generator systems for CSP applications. For instance, an exergonomic analysis was carried out by Gomez-Hernandez et al. [18] to design SGSs for solar tower power plants. Similarly, Lin et al. [19] presented a design procedure and design guidelines for direct steam generation solar tower power plants. The focus towards CSP applications has meant also more interest in the transient performance of such components. The transient performance of SGSs was investigated by Gonzalez-Gomez et al. [20] for solar tower power plants and by Gonzalez-Gomez et al. [21] for PTPP applications, while Mertens et al. [22] compared the transient response during a fast start-up procedure between a natural circulation and a once-through steam generator. In general, the design of each of the SGS components is a key aspect when analysing the steam generator system.

The design of the heat exchangers used in the energy system is characterized by two steps, the heat transfer area estimation and pressure drop calculations coupled with a cost analysis. One of the most common methods to size the shell and tube heat exchangers is the Delaware method for shell-side calculations, which takes into account the different fluid flow paths in the complex shell geometry [23]. Another available method in literature is the Stream Analysis method, which is also implemented in the commercially available software HTRI (Heat Transfer Research, Inc.) [24]. However, if the shell geometry is not too complex, the method proposed by Kern [25] can be used to obtain a good approximation of the area requirements. Considering tube banks, the method summarized by Anarratore et al. [26] can be applied to modify the logarithmic mean temperature based on the tube configurations. Regarding the cost estimation, both simplified [27] and more detailed methods are available. Concerning the latter, Purohit [28] proposed a method to estimate the cost of the heat exchangers not only based on the area requirements, but also on many other factors such as operating pressure, tube configurations and shell sizes.

In literature, different sizing methodologies are applied to different cases. For instance, Duran et al. [29] applied a genetic algorithm to optimize the geometric design of heat recovery steam generators (HRSG). However, the focus was only on the geometrical design and not on the economic analysis. A similar approach is presented by Franco et al. [30], and in this case a two-step optimization approach is presented, by firstly minimizing pressure drops and secondly minimizing the dimension of the heat exchangers. As for the associated cost, for instance, Wildi-Tremblay and Gosselin [31] used a genetic algorithm to minimize both investment and operational costs. Gonzalez-Gomez et al. [32] applied a cost-based optimization methodology to find a trade-off between levelized cost of electricity and investment costs for the SGS specifically for parabolic trough power plant applications.

A general conclusion is that many design methodologies are available and applied in literature, but none so far have taken into consideration the LCF limitations during the design phase. In previous works, the LCF constraints were evaluated as a performance check afterwards by calculating what is the maximum allowable heating rate for a specific given design. For instance, Pelagotti et al. [14] analyzed the lifetime of the header and coil steam generator for a given design. A more detailed approach was performed by Gonzalez-Gomez et al. [10] who estimated the lifetime of the heat exchangers according to the ASME boiler pressure vessel code (BPVC) div. II for a given geometry and assumed heating rates. However, as concluded in a previous work by the authors [6], it is essential to include the heating rates in the design procedure. Increasing the evaporator heating rates from 3 K/min to 7–10 K/min leads to an increase in the electricity production between 1.5% and 5% for a peak-load case.

The objective of this paper is to present a method to design the SGS

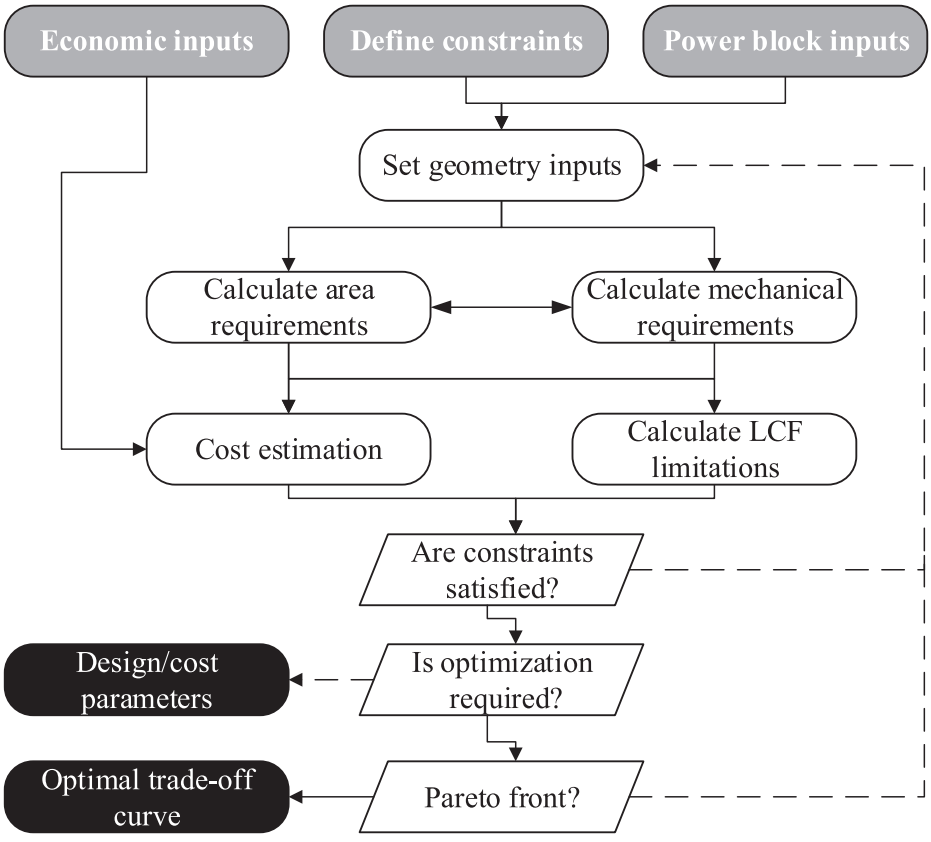


**Fig. 1.** SGS design method workflow. Solid lines represent a YES flow while dashed lines represent a NO flow.

taking into account LCF constraints for concentrating solar power applications. The significance of the results is demonstrated by comparing the results with those of a design which was obtained without considering the LCF constraints.

The thermodynamic and economic calculations were coupled in a multi-objective optimization framework aiming at minimizing both pressure drops and purchase equipment costs (PEC) and considering LCF constraints as obtained from Ref. [6]. The header and coil design was chosen as it is a promising solution for CSP applications. The numerical models were validated with data provided by a manufacturer of a 55 MWe PTPP without storage. In order to show the relevance for a practical application, the proposed design method was applied to the requirements of the mentioned power plant. This is the first paper presenting a method for incorporating the low-cycle fatigue requirements in the design procedure of steam generator systems.

Section 2 below presents the methods used to calculate the required heat transfer parameters and pressure drops as well as the cost estimation and LCF heating rate calculations. Section 2 also contains the multi-objective optimization method and required constraints in order to obtain feasible solutions. Section 3 presents and discusses these findings of the validation and multi-objective optimization performed for two different cases in order to compare the results with the results obtained for the case without accounting for LCF constraints. Section 4 outlines the conclusions and final remarks.

## 2. Methods

Fig. 1 illustrates the main steps that are required for the design routine. The grey and black boxes represent the inputs and outputs of the model, respectively.

In order to perform the SGS design, power block data and operating constraints are the required inputs, together with price data if economic calculations are to be done. The results of the design serve for the LCF analysis according to the norm EN12952-3 [12]. If the constraints are not met, the geometry inputs are changed until the requirements are satisfied.

If the geometrical configuration is already known, the tool can proceed with the design routine. Otherwise, the tool allows for coupling with a multi-objective optimizer available in the Matlab toolbox [33]. At the start of the optimization, it is possible to set conflicting objectives with regards to whether to maximize or minimize their quantities. Both design parameters and operation parameters can be set to allow for variations within the limits chosen for the study. The algorithm performs then as many iterations as needed to finalize the optimization and obtain an optimal trade-off curve or Pareto front [34].

### 2.1. Case study

The power plant of the case study is based on a PTPP similar to the Andasol 1, located near Sevilla [35]. The main difference is the absence of the thermal energy storage and the arrangement of the re-heaters, as in this case the RH is split into two heat exchangers parallel to the economizer (RHe) and the superheater (RHs). The twofold split of the re-heater allows for lower temperature gradients on the tubes, thus resulting in lower thermal stresses [36]. Fig. 2 illustrates a diagram of the reference power plant and the arrangement of the heat exchangers in the system.

The red lines represent the HTF (Therminol-VP1) loop, which is heated up by the parabolic trough (PT) mirrors and fed directly to the steam generator system. The blue line cycle represents a regenerative Rankine-reheat cycle with high pressure (HP) and low pressure (LP) steam turbines (ST), a condenser and a deaerator (D). The main inputs required for defining the boundary conditions of the SGS are summarized in Table 1.

The SGS consists of two parallel trains which comprise a SH, ECO, EVA and two RHs [32]. The heat transfer fluid flows on the shell-side in the single phase heat exchangers. In the evaporator the heat transfer fluid flows in the tube-side, while the heat transfer is characterized by pool boiling on the shell-side. The water flows in the tubes for all the other heat exchangers. The blue and red lines represent, respectively, the water and heat transfer fluid flows. The HTF flows through the SGS to supply the thermal energy to increase the temperature of the inlet subcooled water to the desired turbine inlet temperature. The low pressure steam, coming from the extraction, is heated up in the two re-heaters to the desired re-heat turbine inlet temperature.

To reduce both the dimensions of the HTF header and the EVA shell,

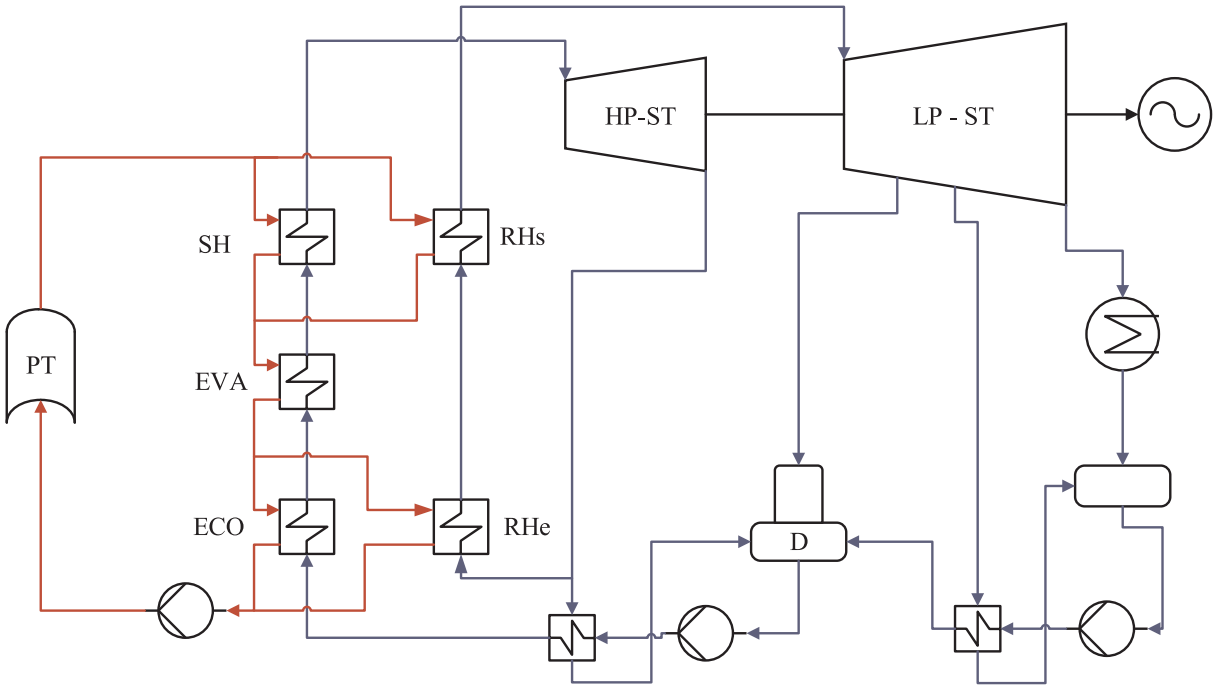


**Fig. 2.** Parabolic trough power plant layout.

**Table 1**
Power block boundary conditions.

| Parameters | Units | Value |
|---|---|---|
| Turbine inlet temperature | [°C] | 385.34 |
| Turbine inlet pressure | [bar] | 104 |
| Reheat outlet temperature | [°C] | 386.46 |
| Inlet pressure at reheat | [bar] | 20.25 |
| Inlet temperature at reheat | [°C] | 213 |
| Feedwater temperature | [°C] | 256.8 |
| HTF inlet temperature | [°C] | 393.3 |
| HTF inlet pressure | [bar] | 15 |
| Heat load requirement | [MW] | 166.2 |

the heat exchanger was split in two. The EVA is characterized by a natural circulation arrangement between the steam drum and the heat exchangers. Fig. 3 illustrates the geometrical configuration of the evaporator under consideration. Fig. 4 shows the single phase heat exchanger geometry, which was approximated as parallel tube banks as illustrated in Fig. 5, where $S_l$, $S_t$, $N_{tl}$ represent the tube longitudinal and transversal pitch and the number of tube layers, respectively. The tubes are fixed in horizontal positions in order to avoid vibration and bending in the transversal direction.

### 2.2. Heat transfer and pressure drops in the heat exchangers

Once the heat duty of the heat exchangers and their boundary conditions are obtained, the mean logarithmic temperature difference (LMTD) is calculated according to Eq. (1) and depends on the inlet (i) and outlet (o) temperature ($T$) of the cold and hot streams. $F$ is a correction factor which depends on the flow configuration. Anarratore et al. [26] suggested, however, that if the number of tube coils is higher than 6, the flow configuration can be assumed to be a counter-current; therefore $F$ becomes 1. The area ($A$), defined in Eq. (3), is calculated by using the overall heat transfer coefficient ($U$) as defined in Eq. (2).

$$\Delta T_{LMTD} = F \cdot \frac{(T_{i,hot} - T_{o,cold}) - (T_{o,hot} - T_{i,cold})}{(\ln((T_{i,hot} - T_{o,cold})/(T_{o,hot} - T_{i,cold})))} \quad (1)$$

$$Q = U \cdot A \cdot \Delta T_{LMTD} \quad (2)$$

$$A_o = N_{tl} \cdot N_{txl} (pi \cdot OD \cdot L_{tube}) \quad (3)$$

$$\frac{1}{U_o} = \frac{r_o}{r_i \cdot h_i} + \frac{1}{h_o} + \frac{r_o \cdot ln\left(\frac{r_o}{r_i}\right)}{\lambda_w} \quad (4)$$

The area depends on the number of tubes for each layer (txl) and tube layers, as well as on the single tube length ($L$). The $U$ value, as expressed in Eq. (4), depends on the heat transfer coefficients $h$ of both shell and tube sides, the internal and the outer radius ($r$), as well as on the thermal resistance posed by the tubes which depends on the wall (w) thermal conductivity ($\lambda$). In the case of the single phase heat exchangers, the tube (water) and the shell (HTF) side heat transfer coefficient were calculated using the Gnielinski [37] and Zukauskas [38] correlations, respectively. In the case of the evaporator, the pool boiling heat transfer coefficient was determined using the Stephan-Abdelsalam correlation [39]. The convective effects on the evaporator water side heat transfer coefficient was considered negligible due to the low water velocities involved (lower than 0.1 m/s). This assumption is also supported by the fact that the heat transfer performance is governed primarily by the heat transfer coefficient on the oil side. Furthermore, the fouling factors were considered negligible. In fact, the manufacturer of such steam generator design guarantees no fouling [36].

Pressure drops on the shell-side were estimated according to the Zukauskas correlation, which takes into account the effective fluid area flow inside the tube layer and is dependent on the number of tube layers the fluid needs to cross [38].

The resulting tube pressure drop can be expressed as the sum of the friction loss on the equivalent length which also takes into account the bend radius and the resulting pressure drop due to the change of direction, normally expressed in terms of a bend-loss coefficient $k_b$. This coefficient depends on the curvature ratio and the bend angle and is obtained according to Idelchik et al. [40]. Eq. (5) presents the calculation of the pressure drop where $\rho$ and $u$ are the density and the velocity of the fluid, and $\theta$ and $R_b$ are the angle and the radius of the bend. Lastly, $f_D$ is the Darcy friction factor which was calculated according to the Colebrook equation for the turbulent regime and to the Poiseuille equation for the laminar regime [37].

$$\Delta P_f = \frac{1}{2} f_D \rho u^2 \left( \frac{\theta R_b + L_{tube}}{ID} \right) + \frac{1}{2} k_b \rho u^2 \quad (5)$$

The driving pressure of the natural circulation mechanism results from the difference in density between the two-phase mixture in the

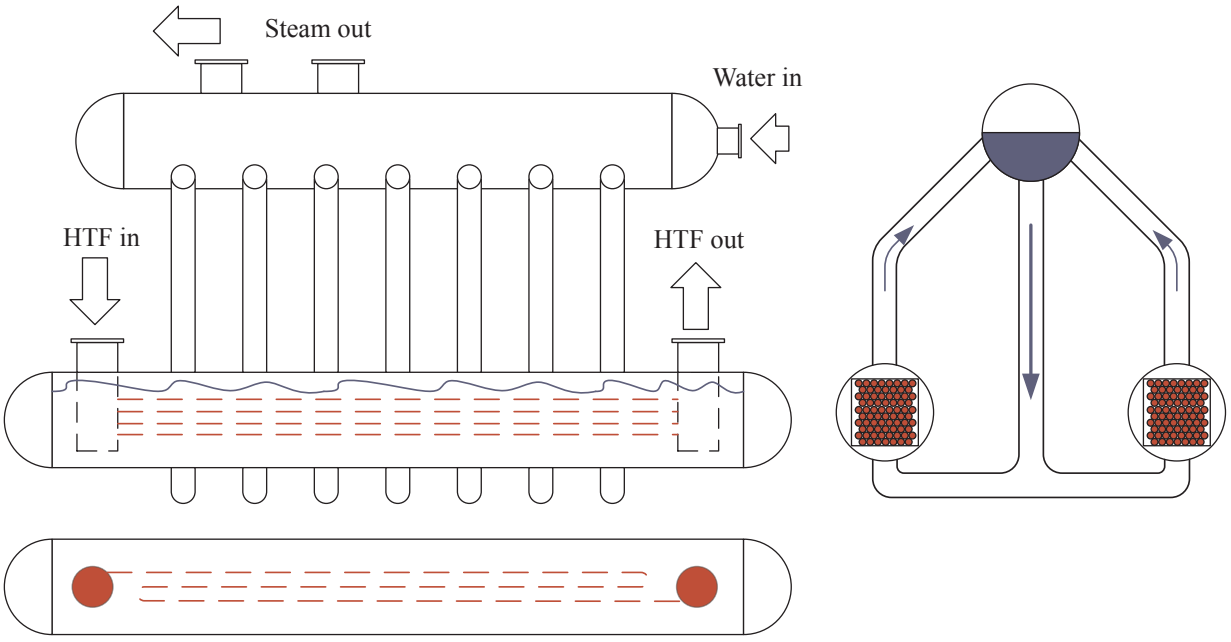


**Fig. 3.** Header and coil shell recirculation evaporator.

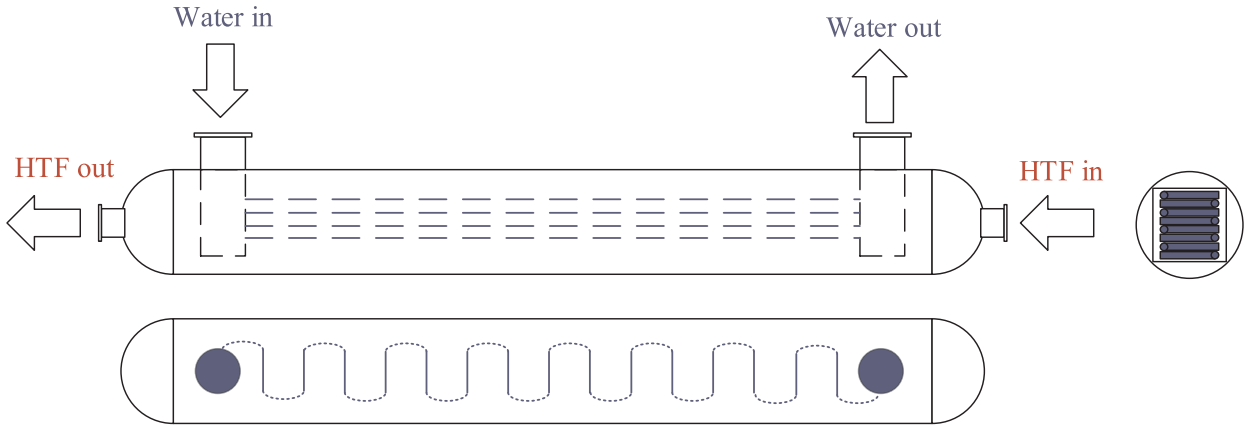


**Fig. 4.** Header and coil shell single phase heat exchanger geometry.

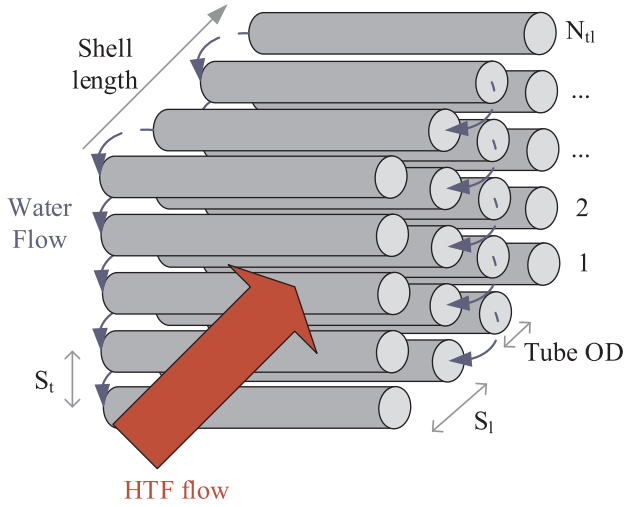


**Fig. 5.** Tube bundle geometry approximation.

riser and the downcomer tubes [41]. For a given circulation ratio (CR) the resulting tube height ($H$) is obtained when the driving pressure (dp) equals the frictional and momentum (fm) pressure losses in the natural circulation circuit (downcomer (dc), riser (r) and heat exchangers (hx)). This was calculated according to Eqs. (6) and (7). Each pressure drop term is calculated according to Anarratore et al. [42].

$$\Delta P_{dp} = g\rho_{dc}H_{dc} - g(\rho_{hx}H_{hx} + \rho_r H_r) \tag{6}$$

$$\Delta P_{fm} = \Delta P_{dc} + \Delta P_r + \Delta P_{hx} + \Delta P_{nozzles} + \Delta P_b \tag{7}$$

### 2.3. Mechanical and geometrical design

The ASME boiler pressure vessel code (BPVC) provides the norms and regulations for calculating the thickness of the shell, headers and tubes in the heat exchangers, which are made of carbon steel material [43].

The shell diameter of each heat exchanger depends on the geometry of the tube bundle, meaning the number of tube layers and the number of coils of the proposed design. In order to minimize the space required by the shell, the length of each coil was calculated to have a square geometry which can be placed inside the shell with a low space waste. Therefore, the internal diameter was determined based on the tube-side geometry, and subsequently the thickness of the shell was calculated according to the BPVC sec. VIII using Eq. (8). The thickness $t$ is dependent on the maximum allowable stress ($S$) of the chosen material at design temperature, design pressure $p$ (in barg) and a safety coefficient $y$. The equation takes into account a tolerance for allowable corrosion ($C$) which usually depends on the material and on the fluid as well as on the requirements of the power plant operator.

$$t_{Shell} = \frac{p \cdot ID/2}{S - (1 - y)p} + C \tag{8}$$

A similar approach was adapted for each pipe (like the headers and risers/downcomers) and tube that are included in the geometry of each heat exchanger. The header diameter was calculated in order to align each tube equidistantly in each layer of the tube bundle geometry. Then the thickness was calculated according to Eq. (9), which depends on the outer diameter ($OD$) of the pipes. Eq. (10) refers to the tube thickness calculation.

$$t_{Tubes} = \frac{p \cdot OD}{2S + p} + 0.005 \cdot OD + C \tag{9}$$

$$t_{Pipes} = \frac{p \cdot OD}{2S + 2y \cdot p} + C \tag{10}$$

In the case of the evaporator heat exchangers, the tube thickness was not calculated directly, as the highest pressure is on the shell and not on the tube side. For externally loaded tubes, the calculation procedure starts by assuming a tube length and thickness, followed by a calculation of the maximum allowable pressure. The iteration stops when this value is higher than or equal to the design pressure considered.

The steam drum volume depends on the operating pressure and on the steam load required by the evaporator. The steam volume chamber was determined according to charts that illustrate the minimum and maximum steam volumes as a function of the operating pressure according to Anarratore et al. [42]. These charts were digitized and the data were obtained using linear interpolation during the optimization. The volume was determined to ensure that the maximum vapor velocity that allows gravitational settling of entrained liquid is not exceeded [42]. Considering that usually the water level corresponds to the center line of the drum, the drum volume becomes twice as large as the required steam drum chamber. According to industrial experience, the internal drum diameter was set to a minimum value of 1.5 m in order to allow for the correct placement of the separating devices and space requirement for internal inspection.

### 2.4. Heating rate calculations

The maximum allowable heating rates ($\nu_T$) were determined according to the European standard EN 12952-3, in order to keep the resulting stress in the singularities (i.e. junction between downcomer and steam drum or header and tubes) below the allowable stress ($\sigma_a$) determined from a LCF diagram for a given number of cycles corresponding to the chosen lifetime of the component [12]. The norm can

be applied to both steam drum/downcomer [7] and header/tubes junctions [44,45]. Eq. (11) summarizes the concept and illustrates how the resulting total stress is a sum of the thermal stress and tensile stress. They depend on thermal and mechanical stress concentration factors, respectively ($\alpha$), which were calculated according to the norm. $E$, $\beta$, and $\nu$ are the Young's modulus, thermal expansion coefficient and Poisson's ratio, respectively. The main non-dimensional parameter is $\Phi_w$ which depends on the outer to inner diameter ratio $\omega$ according to Eq. (12).

$$\left|\alpha_m(p-p_0)\frac{ID+t}{t}+\alpha_T\cdot c\cdot\rho\frac{E\cdot\beta}{1-\nu}\frac{\nu_T t^2}{\lambda}\Phi_w\right|\leqslant|\sigma_a| \tag{11}$$

$$\Phi_w=\frac{1}{8}\frac{(\omega^2-1)(3\omega^2-1)-4\omega^4\cdot ln\omega}{(\omega^2-1)(\omega-1)^2} \tag{12}$$

The norm provides the allowable rates at the corresponding minimum and maximum pressure $p_1$ and $p_2$ in the specified start-up cycle. Once the two values are determined, the heating rate can be calculated at each intermediate pressure by means of linear interpolation according to Eq. (13). In the case of two-phase conditions, the pressure p(t) becomes a function of the fluid temperature $T_f$; therefore, the equation was solved using a fourth-order Runge-Kutta method [46]. Otherwise, the pressure is a function of time and the equation can be directly solved [7]. The minimum and maximum heating rates do not, however, illustrate the overall start-up process as $\nu_T$ changes during the start-up phase. In order to capture the overall responsiveness of the start-up procedure, an average heating rate was defined according to Eq. (14). The heating rates were also calculated for a specific start-up cycle, which was obtained from the results of a parabolic trough model, previously developed by the authors [6]. The chosen lifetime equals 25 years, with 346 starts in a year of which there were 91 hot, 234 warm and 21 cold starts which would respectively correspond to a starting pressure of 26 bar, 16 bar and 1 bar, respectively.

$$\frac{dT_f}{dt}=\frac{p_2\cdot\nu_{T1}-p_1\cdot\nu_{T2}}{p_2-p_1}+\frac{\nu_{T2}-\nu_{T1}}{p_2-p_1}\cdot p(t) \tag{13}$$

$$\nu_{Taverage}=\frac{1}{t_{end}-t_{start}}\cdot\int_{t_{start}}^{t_{end}}\frac{dT_f}{dt}\,dt \tag{14}$$

### 2.5. Cost estimation

The cost estimation of the whole SGS was carried out following the method presented by Purohit et al. [28]. The method is based on estimating the cost of a baseline exchanger according to Eq. (15), where $p_{OD}$, $f$ and $r$ are cost multipliers for the outer diameter, front and rear head types, respectively. The total heat exchange cost was then determined as a function of the heat exchange area according to Eq. (17), where $N_s$ represents the number of shells and $c_{i,j}$ represent a number of correction factors which take into account design pressure, length of the tubes and material selection. The cost of the steam drum was estimated as a function of the drum metal mass [47] and carbon steel prices according to Ref. [48]. Lastly, the total investment cost was adjusted to 2017 as a reference year according to the historical price index (*HPI*) reported in Ref. [49].

$$b=\left(\frac{6.6}{1-e^{\left(\frac{7-ID}{27}\right)}}\right)\cdot p_{OD}\cdot f\cdot r \tag{15}$$

$$PEC_{hx}=b\cdot\left(1+\sum_{i=1}^{n}c_i\right)\cdot A\cdot N_s \tag{16}$$

$$PEC_{SGS}=\frac{HPI_{2017}}{HPI_{1983}}\cdot\sum_{j=1}^{n_{hx}}\left(b_j\cdot\left(1+\sum_{i=1}^{n}c_{i,j}\right)\cdot A_j\cdot N_{s,j}\right) \tag{17}$$

### 2.6. Optimization and constraints

Apart from the investment cost, another important parameter to consider during a heat exchanger feasibility study is the pressure drop of both fluids. The lower the pressure drop, the higher the heat exchanger area required as lower heat transfer coefficients are obtained. Therefore, investment cost and pressure drops are conflicting parameters. Moreover, from a system perspective, higher mass flow rates from the HTF side would imply higher parasitic consumptions and therefore lower profitability of the power plant. Lastly, if the CSP plant includes TES systems, lower outlet HTF temperatures would allow for a lower cost on the thermal energy storage. Gonzalez-Gomez et al. [32] included all these considerations in their cost analysis; however, as the focus of this paper is to look into the details of just the SGS, only the minimization of the pressure drop and PEC was considered. Secondly, it is common practice in industry to ask the manufacturer of SGSs for a system of heat exchangers for certain fixed power plant specifications and maximum allowable pressure drop. Hence having a trade-off curve between pressure drop and PEC, would allow to choose the most cost-effective design for a set of power plant constraints.

The optimization was carried out with the genetic algorithm multi-objective optimization toolbox available in Matlab by varying the parameters as presented in Table 2. It was decided to choose the same tube outer diameter for each heat exchanger, to favor an economy of scale. The diameter was chosen to be a discrete variable, with the possibility to choose from four different commonly available tube outer diameters according to Coulson et al. [50]. The four choices (referred to as index in Table 3) were 25 mm, 30 mm, 38 mm and 50 mm, respectively, with lower diameters excluded from the optimization since these designs gave rise to high pressure drops (above 10 bar). The tube pitch values were chosen to be fixed to the lowest value allowable by not drastically increasing the pressure drops. This resulted in a tube pitch ratio (distance/diameter) of 1.25 and a staggered alignment to allow for the lowest shell diameters, higher heat transfer coefficient and easy mechanical cleaning [25,51]. These choices are also in agreement with the results presented by Gonzalez-Gomez et al. [32].

In order to allow the optimization algorithm to obtain feasible designs, constraints were set according to Table 3. The minimum and maximum tube side velocities were set in order to reduce possible fouling and avoid excessive corrosion, respectively [50]. The maximum steam flow velocities, which are dependent on operational pressure, were set according to the steam velocity diagram presented by Merritt et al. [52].

The constraints also took into consideration the minimum heating rates for each component (header/tube junction for single phase heat exchangers and drum/downcomer junction for the evaporator). As the evaporator is the main limiting component for the SGS, a minimum heating rate was chosen according to a previous work by the authors [6]. This value was chosen to maximize the electric power output of the

**Table 2**
Optimization decision variables.

| Variables | Unit | Lower boundary | Upper boundary |
|---|---|---|---|
| Tube outer diameter index | [–] | 1 | 4 |
| RHe number of layers | [–] | 20 | 40 |
| RHs number of layers | [–] | 20 | 40 |
| EVA number of layers | [–] | 20 | 40 |
| SUP number of layers | [–] | 20 | 40 |
| ECO number of layers | [–] | 20 | 40 |
| Rhe number of tubes per layer | [–] | 3 | 15 |
| RHs number of tubes per layer | [–] | 3 | 15 |
| EVA number of tubes per layer | [–] | 3 | 15 |
| SUP number of tubes per layer | [–] | 3 | 15 |
| ECO number of tubes per layer | [–] | 3 | 15 |
| Riser outer diameter | [mm] | 200 | 300 |
| Number of risers | [–] | 5 | 15 |

**Table 3**
Optimization constraints.

| Parameter | Unit | Value |
|---|---|---|
| Tube minimum velocity | [m/s] | 0.5 |
| Tube maximum velocity | [m/s] | 4 |
| Shell minimum velocity | [m/s] | 0.2 |
| Shell maximum velocity | [m/s] | 1.5 |
| Steam maximum velocity | [m/s] | 25 |
| Oil maximum pressure drop | [bar] | 2 |
| Evaporator minimum heating rate | [K/min] | 8.5 |
| Super-heater minimum heating rate | [K/min] | 15 |
| Minimum drum internal diameter | [mm] | 1500 |

power plant. All the other components were checked to have a lifetime higher than or equal to 25 years. The optimization was carried out for the following two cases:

1. No LCF constraints
2. LCF constraints, with minimum heating rate for both the evaporator and superheater

Other constraints, which specifically apply only to the evaporator, were related to limiting the maximum heat flux for the tube bundle to avoid film boiling [53,54] and assuring that the critical flow $G_c$ in the water-steam mixture is not reached. This was estimated according to Eq. (18), in which the reference (ref) properties were calculated at the upstream stagnation point (steam drum) and $c_f$ is a choking correction factor [55].

$$G_c = \sqrt{2 \cdot [p_{ref} - c_f \cdot p_{sat} \cdot (T_{ref})] \cdot \rho_{l,ref}} \quad (18)$$

## 3. Results and discussion

### 3.1. Model validation

A steady state validation was performed by comparing the most significant outputs of the model with data of the SGS of an existing 55 MWe parabolic trough power plant employing a header and coil steam generator. Table 4 summarizes the validation of the key parameters of the design routine. As the detailed geometrical design of the components considered for evaluating the accuracy of the model is confidential, only the main results are presented here. The total area required by each heat exchanger is in line with the plant data with a deviation of +2.5%, meaning that the model is able to predict the heat transfer coefficients with a reasonable degree of accuracy. This is also reflected in a deviation below 1% for the total HTF temperature drop. The small deviations in outlet velocities of water and HTF indicate that the pressure drops on each fluid side are estimated with good accuracy.

The Purohit method used for the SGS cost estimation was developed specifically for the TEMA configuration, but in the case of the header and coil geometry, its applicability was demonstrated by comparing its results with cost figures provided by the boiler manufacturer. For the different sizes provided, the relative deviations between the results of the cost model and the manufacturer data were below 2%, justifying the use of the method also for the header and coil geometry. Furthermore, the results shown in Table 4 indicate that even though the area is overestimated, the weight experiences an opposite trend. This can be explained by the fact that the thicknesses of the components are underestimated with an average of 2.9%. This is related to the fact that a manufacturer would choose a tube with the closest dimensions in terms of thickness and diameter among those available on the market. In conclusion, the results of the validation suggest that the models provide sufficiently accurate results for the purpose of the work presented in this paper.

### 3.2. Optimization results

The multi-objective optimization results are presented in Fig. 6. Fig. 6a presents a comparison of the results when excluding (Case 1) and including the LCF constraints (Case 2), see Section 2.6. Fig. 6b presents the optimization results with the HTF total pressure drop as color. If the main thermodynamic constraints are considered (Case 1), the 25 mm outer diameter solution is excluded as the pressure drop and velocity constraints (HTF/water) are not met. Therefore, only the other three diameters of 30 mm, 38 mm and 50 mm (from left to right) are feasible tube diameter options. If the LCF constraints are considered with a required minimum heating rate for the evaporator (Case 2), the 30 mm outer diameter is excluded for two reasons. In the case of a low tube number (towards the lower limit), the pressure drop on the SH side would increase significantly, meaning a higher steam pressure requirement at the drum, if the turbine inlet pressure is considered to be constant. This would require higher thicknesses on both the drum and downcomer tubes, increasing thermal stresses and lowering the maximum allowable heating rates. If the superheater tube number would be increased, the header diameter would need to be increased. This would mean higher thickness requirements; therefore, the superheater header would experience higher thermal stresses and hence the LCF constraints would not be satisfied at the superheater tube/header junction. In order to include the 30 mm outer diameter solution the evaporator heating rate constraint would need to be lowered to 6 K/min, hence making the design not optimal from a system perspective.

If a tube diameter of 50 mm for all the heat exchangers is considered, for the same pressure drop the design would change with an associated increase in PEC. For instance, for 0.1 bar pressure drop this would result in a 7.6% increase in the PEC. This is due to the fact that in order to keep low pressure drops as well as meeting the LCF constraints, more layers would be required resulting in higher shell diameters. This would in turn increase the cost for the superheater.

Fig. 6a also illustrates that in order to obtain a desired pressure drop, the design could drastically change if the LCF constraints are considered during the design procedure. For instance, if a 1 bar pressure drop is required, the PEC would increase by around 0.75 million USD, while increasing the LCF constraint from 6.2 K/min (Case 1) to 9.1 K/min (Case 2). Even though this figure corresponds to a 42% increase in capital cost of the SGS, it is justifiable if the economy of the whole power plant is taken into consideration.

According to a previous work of the authors [6], an evaporator $\nu_T$ increase from 6.2 K/min to 8.5 K/min would imply an increase in electricity production which would range between 0.84% and 3.31%, with the highest value in the case the superheater is optimally designed and operated considering the heating rate perspective. In a 25-year lifetime of the plant, and even assuming the lowest bid for CSP power production of 94.5 USD/MWh [56], this could result in an increase in revenues of between 1.17 million USD and 4.7 million USD. If there were different designs where only low heating rate constraints (3 K/min) were employed, the, these figures could rise to 2.1 million USD and 7.1 million USD, respectively.

The optimal geometrical parameters for Case 2 for different

**Table 4**
Validation results.

| Parameters | Units | Model | Plant data | Deviation |
|---|---|---|---|---|
| Total area required (HTF side) | [$m^2$] | 2755 | 2688 | 2.50% |
| HTF SGS temperature drop | [K] | 92.40 | 91.70 | 0.76% |
| Pressure drop (HTF side) | [bar] | 1.663 | 1.640 | 1.40% |
| Pressure drop (Water side) | [bar] | 1.850 | 1.852 | −0.11% |
| Velocity SH steam outlet | [m/s] | 10.81 | 10.95 | −1.32% |
| Velocity ECO HTF outlet | [m/s] | 0.912 | 0.900 | 1.33% |
| EVA maximum heating rate | [K/min] | 8.830 | 9.000 | −1.89% |
| Total weight | [ton] | 231.8 | 240.4 | −3.59% |

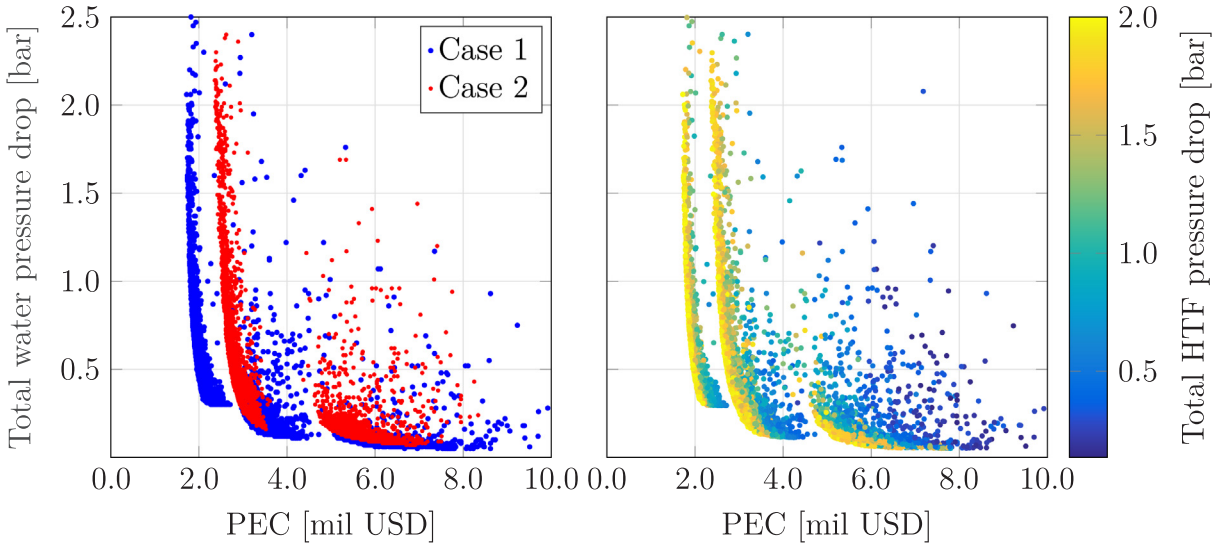


(a) Comparison between the two cases (b) HTF total pressure drop

**Fig. 6.** Optimization results.

conditions are presented in Table 5. It lists the arithmetic mean average, relative standard deviation (RSD) around the mean, and minimum and maximum values of the optimized variables at the Pareto front. In order to give an indication of feasible designs for different pressure drops, the table is split between pressure drops higher and lower than 1 bar for the solution corresponding to a tube outer diameter of 38 mm. A third column is presented for the 50 mm solution, which corresponds to pressure drops lower than 0.225 bar.

A low RSD and small difference between minimum and maximum values mean that the corresponding variable does not vary significantly within the optimal configuration. The EVA, ECO, SH number of layers and EVA tubes per layer present the lowest RSD for pressure drops higher than 1 bar. Similar conclusions can be drawn for designs which would result in lower pressure drops. The results presented for the number of tube layers for the superheater support the aforementioned discussion regarding the necessity to increase such parameter in cases where low pressure drops are required. The third column shows that in this case, an increase by 28% is necessary to satisfy this condition.

It may also be noticed that the riser configuration (outer diameter and numbers) presents a low RSD. Low number of risers would imply higher pressure drops, therefore larger height values for both downcomers and risers. Larger diameters would imply lower velocities and hence lower pressure drops, but higher required thicknesses. The results presented in the three columns can be interpreted as the optimal configuration, considering the trade-off between the number of tubes and diameter to minimize thickness and height and hence the associated cost. The differences among the three columns are due to the different operating pressure at the evaporator (due to higher pressure drops at the superheater), thus leading to different optimal configurations.

The difference in optimal diameter for the high pressure drop designs is the most evident change between the two cases. Table 6 presents a comparison in terms of relative change in the number of tubes among the optimal designs for the pressure drop ranges as presented in Table 5. The average values for the whole Pareto front are presented in an additional column. Each column presents the relative variation of tube numbers in Case 2 as compared to Case 1. The variation stems from either an increase in number of tube layers or number of tubes for each layer. The main trend is an overall increase in number of tubes for each heat exchanger. The superheater presents the highest relative increase in number of tubes both for the high pressure drop designs and as an average considering the whole pressure drop range. By lowering the water pressure drop, the economizer presents the highest increase. In this case, in order to lower further the water side pressure drop and at the same time keep high maximum allowable heating rates, the economizer pressure drop is decreased by increasing its number of tubes in equal proportion between number of layers and number of tubes for

**Table 5**
Optimization results for Case 2. Minimum, mean, maximum and relative standard deviation of the optimized variables. The values are acquired from the Pareto front in Fig. 6a.

| Variables | Units | Higher than 1 bar | | | | Between 0.225 and 1 bar | | | | Lower or equal to 0.225 bar | | | |
|---|---|---|---|---|---|---|---|---|---|---|---|---|---|
| | | min | mean | max | RSD | min | mean | max | RSD | min | mean | max | RSD |
| Tube outer diameter | [mm] | 38 | 38 | 38 | 0% | 38 | 38 | 38 | 0% | 50 | 50 | 50 | 0% |
| RHe number of layers | [–] | 28 | 29 | 30 | 3% | 28 | 32 | 39 | 10% | 27 | 34 | 38 | 9% |
| RHs number of layers | [–] | 31 | 34 | 36 | 5% | 34 | 35 | 35 | 1% | 28 | 34 | 40 | 8% |
| EVA number of layers | [–] | 29 | 30 | 33 | 4% | 21 | 23 | 29 | 7% | 20 | 20 | 22 | 3% |
| SH number of layers | [–] | 20 | 22 | 24 | 6% | 21 | 25 | 29 | 6% | 25 | 32 | 39 | 13% |
| ECO number of layers | [–] | 21 | 23 | 26 | 6% | 21 | 22 | 29 | 6% | 20 | 21 | 29 | 9% |
| RHe number of tubes per layer | [–] | 7 | 8 | 10 | 14% | 8 | 11 | 13 | 10% | 14 | 15 | 15 | 3% |
| RHs number of tubes per layer | [–] | 7 | 8 | 9 | 11% | 8 | 11 | 15 | 18% | 14 | 15 | 15 | 3% |
| EVA number of tubes per layer | [–] | 4 | 4 | 4 | 0% | 4 | 5 | 5 | 4% | 3 | 3 | 5 | 21% |
| SH number of tubes per layer | [–] | 4 | 6 | 7 | 18% | 7 | 10 | 11 | 10% | 8 | 8 | 11 | 12% |
| ECO number of tubes per layer | [–] | 5 | 6 | 7 | 12% | 5 | 6 | 8 | 13% | 6 | 7 | 8 | 9% |
| Riser outer diameter | [mm] | 253 | 280 | 296 | 5% | 261 | 293 | 300 | 3% | 294 | 298 | 300 | 1% |
| Number of risers | [–] | 5 | 6 | 7 | 10% | 5 | 6 | 8 | 9% | 5 | 6 | 8 | 8% |

**Table 6**
Comparison of designs of the two optimization cases (Case 2 compared with Case 1) in terms of relative change in the number of tubes for each heat exchanger.

| Component | $p > 1$ bar | 0.225 bar $< p \leq 1$ bar | $p \leq 0.225$ bar | Average |
|---|---|---|---|---|
| RHe | 145.0% | 134.1% | 105.6% | 128.2% |
| RHs | 141.5% | 132.8% | 110.4% | 127.9% |
| EVA | 105.0% | 134.8% | 127.6% | 122.1% |
| SH | 154.8% | 145.0% | 125.6% | 141.8% |
| ECO | 121.8% | 156.1% | 131.7% | 136.5% |

each layer. Both Fig. 6a and Table 6 suggest that by including LCF constraints during the design phase, different optimal designs are obtained in the whole cost range, with the cheaper designs being the most affected.

Table 7 illustrates the results of the optimized geometry for a 1 bar pressure drop on the water side. The header diameter results support the aforementioned observations concerning the number of tubes. Low numbers are preferred in the high pressure heat exchangers, while large header diameters are preferred on the re-heater train side. The two most expensive components are the evaporator and superheater, accounting for 34% and 27%, respectively, of the overall PEC. That is also why the optimizer tends to provide a low number of tubes and high heat transfer coefficients for these components. On the other hand, the re-heaters are less sensitive both from a heating rate and an area/cost perspective, accounting for 14% and 12% of the overall PEC. That is why in Table 5, the re-heater parameters experience high variations in the optimal solutions.

In order to minimize the PEC, the HTF total pressure drop converges to the maximum allowable value of 2 bar. That is, if this value decreases, higher costs would be obtained; see Fig. 6b. This is mainly due to the fact that, in order to decrease the shell-side velocity, a lower number of coils would be needed, meaning a higher number of tubes. In turn this would cause low water side velocities, hence an increased heat exchanger area requirement. This would mean that for a water-side 1 bar pressure drop, decreasing the HTF pressure drop from 2.0 to 1.5 bar would result in a PEC increase of 13%.

It needs to be stressed that the results presented in this section are governed by the power plant design specifications. Therefore, if a CSP plant is optimized while employing the method presented in this paper for the SGS design, different optimal SGS designs other than the ones presented here may be obtained, depending on the size of the solar field and thermal energy storage. However, the method presented in this paper can be used to provide guidelines on how to design the SGS for a given set of design specifications and be applied during the pre-design phase of CSP plants to obtain the most suitable design.

The results presented in the paper are specific to the parabolic trough power plants. Even though these plants are the most commercially mature, solar tower plants are experiencing an increasing trend in interest [57]. The methods presented in the paper could be applied in a similar way to solar tower power plants. The main difference would derive from the presence of molten salt as the heat transfer fluid and the associated risk of freezing at relatively high temperature [58]. This would require a different design of the evaporator as the molten salt would be required on the shell-side in order to minimize the freezing risk and facilitate maintenance. Another difference would be the operating temperature. Typically, solar tower plants operate at around 565 °C. Having a higher temperature would require different materials and impose different stress cycles, hence the impact of the LCF constraints is expected to be more pronounced.

## 4. Conclusions

A design tool was developed to size all the heat exchangers of a steam generator system for concentrating solar power applications. The models included the area calculations based on heat transfer coefficients, and sizing of the main components, such as tubes, headers and shells. For the first time a sizing routine was presented including the evaluation of low-cycle fatigue requirements, in terms of maximum allowable heating rates for the most significant components, and its significance was demonstrated by comparison of the results with a design for which thermo-mechanical constraints were not considered. The sizing was also coupled with a cost estimation model. This allows coupling the thermo-mechanical and economic aspect to integrate the model in a genetic algorithm based multi-objective optimization to minimize both pressure drops and purchase equipment cost.

The results of the validation indicate that models provide accurate results, resulting in an overestimation of the total heat exchanger area by 2.5% compared to components installed in existing power plants. The total weight was underestimated by 3.6%. Lastly, the low-cycle fatigue norms were implemented with a resulting deviation in an evaporator heating rate calculation of −1.9% compared to that of the existing power plant.

The results of the multi-objective optimization indicate that

**Table 7**
Result design for 1 bar pressure drop on water side.

| Parameter | Units | ECO | EVA (†) | | SH | RHe | RHs |
|---|---|---|---|---|---|---|---|
| Shell diameter | [mm] | 1636 | 1465 | 1658 | 1709 | 2246 | 2599 |
| Shell length | [mm] | 9.3 | 13.2 | 8.95 | 15.03 | 16.54 | 17.1 |
| Shell thickness | [mm] | 18 | 65 | 79 | 20 | 23 | 29 |
| Number of shells | [–] | 1 | 2 | 1 | 1 | 1 | 1 |
| Tube outer diameter | [mm] | 38 | 38 | | 38 | 38 | 38 |
| Tube thickness | [mm] | 3.8 | 4.8 | | 3.8 | 3.8 | 3.8 |
| Tube layers | [–] | 22 | 29 | | 23 | 30 | 34 |
| Tube per layers | [–] | 6 | 4 | | 7 | 9 | 9 |
| Tube coils | [–] | 23 | 3 | | 34 | 10 | 12 |
| Header diameter | [mm] | 380.6 | 216.4 | | 465.9 | 560.5 | 489.2 |
| Header thickness | [mm] | 27.0 | 22.6 | | 37.0 | 19.0 | 16.0 |
| Tube side average flow velocity | [m/s] | 0.52 | 3.39 | | 6.50 | 18.48 | 17.82 |
| Shell side average flow velocity | [m/s] | 1.01 | – | | 1.04 | 0.59 | 0.52 |
| Tube side heat transfer coefficient | [W/(m$^2$ K)] | 4567.0 | 5311.0 | | 2024.3 | 735.5 | 578.3 |
| Shell side heat transfer coefficient | [W/(m$^2$ K)] | 1993.1 | 23472.7 | | 1866.1 | 1441.3 | 1218.1 |
| Overall heat transfer coefficient | [W/(m$^2$ K)] | 1155.2 | 3245.6 | | 1155.2 | 402.7 | 325.4 |
| Oil side pressure drop | [bar] | 0.289 | 1.133 | | 0.445 | 0.078 | 0.294 |
| Water side pressure drop | [bar] | 0.031 | 0.017 | | 0.472 | 0.294 | 0.206 |
| Purchase equipment cost | [mil USD] | 0.350 | 0.850 | | 0.690 | 0.290 | 0.350 |
| $v_T$ average | [K/min] | 68.7 | 9.1 | | 31.7 | 246.1 | 153.7 |

(†) The shell parameters refer to the heat exchangers (on the left) and steam drum (on the right).

integrating the low-cycle fatigue analysis in the design routine of steam generator systems can change significantly the design of the heat exchangers. If both the superheater and the evaporator minimum heating rate constraints are considered, only two tube outer diameter choices (38 mm, 50 mm) give optimal solutions. If 1 bar water-side pressure drop is a requirement from a power plant owner, the cost of an optimal heat exchanger could potentially increase by 0.75 million USD (42% purchase equipment cost increase). However, considering that high heating rates could lead to an increase in electricity production, the increase in steam generator system cost can be justifiable. The optimization results also suggest that a lower heat transfer fluid total pressure drop constraint implies high purchase equipment costs. Specifically, for the 1 bar water-side pressure drop design, lowering the heat transfer fluid pressure drop from 2.0 bar to 1.5 bar would imply a purchase equipment cost increase of 13%.

The results presented in this work are specifically tailored for one power plant design in order to keep the focus of the work only on the component design. Integrating this methodology in a more general system level optimization may lead to different optimal steam generator configurations depending on the power plant specifications, such as thermal energy storage, solar field size and parasitic consumption.

## References


[1] International Energy Agency. Technology roadmap, solar thermal electricity. Technical report. Paris (France): IEA; 2014.
[2] Mancini Thomas R, Gary Jesse A, Kolb Gregory J, Kuofei Ho Clifford. Power tower technology roadmap and cost reduction plan. Sandia report. Technical report Sandia report. Albuquerque (New Mexico): Sandia, Sandia National Laboratories; 2011.
[3] World Energy Council. World energy resources: solar 2016. Technical report. London, England; 2016.
[4] Groupe Reaction Inc. CSP parabolic trough report: cost, performance and key trends. Technical report. London (England): CSP Today; 2014.
[5] Estela, Greenpeace, and Solarpaces. Solar thermal electricity - global outlook 2016. Technical report. Brussels, Belgium; 2016.
[6] Ferruzza D, Topel M, Laumert B, Haglind F. Impact of steam generator start-up limitations on the performance of a parabolic trough solar power plant. Sol Energy 2018;169:255–63.
[7] Dzierwa Piotr, Taler Jan. Optimum heating of pressure vessels with holes. J Press Vessel Technol 2014;137(1):011202.
[8] Dzierwa Piotr, Taler Dawid, Trojan Marcin, Taler Jan. Evaporator heating with optimum fluid temperature changes. Procedia Eng 2016;157:29–37.
[9] Taler Jan, Weglowski Bohdan, Taler Dawid, Sobota Tomasz, Dzierwa Piotr, Trojan Marcin, et al. Determination of start-up curves for a boiler with natural circulation based on the analysis of stress distribution in critical pressure components. Energy 2015;92:153–9.
[10] Gonzalez-Gomez PA, Gomez-Hernandez J, Briongos JV, Santana D. Fatigue analysis of the steam generator of a parabolic trough solar power plant. Energy 2018;155:565–77.
[11] Duda Piotr, Rzasa Dariusz. Numerical method for determining the allowable medium temperature during the heating operation of a thick-walled boiler element in a supercritical steam power plant. Int J Energy Res 2012;36(6):703–9.
[12] CEN. Water-tube boilers and auxiliary installations - Part 3: design and calculation for pressure parts of the boiler. Technical report. Brussels (Belgium): European Committee for Standardization; 2012.
[13] Vant-Hull LL. Central tower concentrating solar power (CSP) systems. Houston (Texas): Woodhead Publishing Limited; 2012.
[14] Pelagotti Leonardo, Sørensen Kim, Condra Thomas J, Joseph Thomas, Franco Alessandro. Modelling of a coil steam generator for CSP applications. In: Proceedings of the 55th international conference on simulation and modelling; 2014.
[15] Mercati Stefano, Milani Massimo, Montorsi Luca, Paltrinieri Fabrizio. Design of the steam generator in an energy conversion system based on the aluminum combustion with water. Appl Energy 2012;97:686–94. Energy Solutions for a Sustainable World - Proceedings of the Third International Conference on Applied Energy, May 16-18, 2011 - Perugia, Italy.
[16] Liu Chengyang, Yan Changqi, Wang Jianjun. Optimal design of vertical natural circulation steam generator. Nucl Eng Des 2012;252:167–78.
[17] Chen Lei, Yan Changqi, Wang Jianjun. Multi-objective optimal design of vertical natural circulation steam generator. Prog Nucl Energy 2013;68:79–88.
[18] Gómez-Hernández J, González-Gómez PA, Briongos JV, Santana D. Influence of the steam generator on the exergetic and exergoeconomic analysis of solar tower plants. Energy 2018;145:313–28.
[19] Lin Meng, Reinhold Jan, Monnerie Nathalie, Haussener Sophia. Modeling and design guidelines for direct steam generation solar receivers. Appl Energy 2018;216:761–76.
[20] González-Gómez PA, Gómez-Hernández J, Briongos JV, Santana D. Transient thermo-mechanical analysis of steam generators for solar tower plants. Appl Energy 2018;212:1051–68.
[21] González-Gómez PA, Gómez-Hernández J, Ferruzza D, Haglind F, Santana D. Dynamic performance and stress analysis of the steam generator of parabolic trough solar power plants. Appl Therm Eng 2019;147:804–18.
[22] Mertens Nicolas, Alobaid Falah, Starkloff Ralf, Epple Bernd, Kim Hyun-Gee. Comparative investigation of drum-type and once-through heat recovery steam generator during start-up. Appl Energy 2015;144:250–60.
[23] Serna M, Jiménez Arturo. A compact formulation of the Bell-Delaware method for heat exchanger design and optimization. Chem Eng Res Des 2005;83(5 A):539–50.
[24] Serth Robert W, Lestina Thomas G. The stream analysis method. 2nd ed. Boston (Massachusetts): Academic Press; 2014.
[25] Kern DQ. Process heat transfer. Singapore: McGraw-Hill; 1965.
[26] Anarratore Donatello. Handbook for heat exchangers and tube banks design. Milano (Italy): Springer; 2010.
[27] Hall SG, Ahmad S, Smith R. Capital cost targets for heat exchanger networks comprising mixed materials of construction, pressure ratings and exchanger types. Comput Chem Eng 1990;14(3):319–35.
[28] Purohit GP. Estimating costs of shell-and-tube heat exchangers. Chem Eng 1983(90):56–67.
[29] Dolores Durán Ma, Valdés Manuel, Rovira Antonio, Rincón E. A methodology for the geometric design of heat recovery steam generators applying genetic algorithms. Appl Therm Eng 2013;52(1):77–83.
[30] Franco Alessandro, Giannini Nicola. A general method for the optimum design of heat recovery steam generators. Energy 2006;31(15):3342–61.
[31] Wildi-Tremblay Philippe, Gosselin Louis. Minimizing shell-and-tube heat exchanger cost with genetic algorithms and considering maintenance. Int J Energy Res 2007;31(31):135–47.
[32] González-Gómez PA, Petrakopoulou F, Briongos JV, Santana D. Cost-based design optimization of the heat exchangers in a parabolic trough power plant. Energy 2017;123:314–25.
[33] MATLAB, version 9.1.0.4 (R2016b). The Natick (Massachusetts): MathWorks Inc.; 2016.
[34] Basil Leyland Geoffrey, Favrat Daniel. Multi-objective optimization applied to industrial energy problems [Ph.D. thesis]. Lausanne: École Polytechnique Féderale de Lausanne (EPFL); 2002.
[35] NREL. System advisor model (SAM) case study: andasol. Technical report. Aldeire (Spain): NREL; 2013.
[36] Aalborg CSP. http://www.aalborgcsp.com/quickmenu/brochures/ [accessed: 2017-08-03].
[37] Bergman Theodore, Lavine Adrienne, Incropera Frank, Dewitt David. Fundamentals of heat and mass transfer. 7th ed. Jefferson city (Missouri): John Wiley and Sons; 2011.
[38] Žukauskas A. Heat transfer from tubes in crossflow. Adv Heat Transfer 1972;8:93–160.
[39] Stephan K, Abdelsalam M. Heat-transfer correlations for natural convection boiling. Int J Heat Mass Transfer 1980;23(1):73–87.
[40] Idelchik IE. Hanbook of hydraulic resistance. Coefficients of local resistance and of friction. Jerusalem (Israel): National Science Foundation; 1986.
[41] Ganapathy V. Understanding boiler circulation. Chem Eng 2013;120(10):52–6.
[42] Anarratore Donatello. Steam generators. Description and design. Milano (Italy): Springer; 2008.
[43] American society of mechanical engineer. ASME Boiler and Pressure Vessel Code: Section VIII - Division 2, New York, New York; 2015.
[44] Hübel Moritz, Meinke Sebastian, Andrén Marcus T, Wedding Christoffer, Nocke Jürgen, Gierow Conrad, et al. Modelling and simulation of a coal-fired power plant for start-up optimisation. Appl Energy 2017;208:319–31.
[45] Meinke Sebastian. Modellierung thermischer kraftwerke vor dem hintergrund steigender dynamikanforderungen aufgrund zunehmender windenergie- und photovoltaikeinspeisung [M.Sc. thesis]; 2012.
[46] Butcher JC, Wanner G. Runge-Kutta methods: some historical notes. Appl Numer Math 1996;22(1):113–51 Special Issue Celebrating the Centenary of Runge-Kutta Methods.
[47] Seader JD, Seider Warren D, Lewin Daniel R. Product and process design principles: synthesis, analysis and evaluation. USA: Wiley; 2004.
[48] MEPS International. http://worldsteelprices.com/ [accessed: 01/03/2018].
[49] Capital professional services. https://inflationdata.com/ [accessed: 01/03/2018].
[50] Towler Gavin, Sinnott Ray. Heat-transfer equipment. In: Chemical engineering design. Oxford, England; 2013. p. 1047–1205.
[51] Khan Waqar Ahmed, Yovanovich MM, Culham JR. Optimal design of tube banks in crossflow using entropy generation minimization method. J Thermophys Heat Transfer 2007;21(2):372–8.
[52] Merritt Carey. Process steam systems: a practical guide for operators, maintainers, and designers. New Jersey: John Wiley & Sons; 2015.
[53] Palen JW. Shell and tube reboilers. In: Heat exchanger design handbook. Begell House, London, England; 2002.
[54] Kandlikar SG. A theoretical model to predict pool boiling critical heat flux incorporating effects of contact angle and orientation. ASME J Heat Transfer 2001;123(6):1071–9.
[55] Kim Yeon Sik. A proposed correlation for critical flow rate of water flow. Nucl Eng Technol 2015;47(1):135–8.
[56] New energy update. http://analysis.newenergyupdate.com/csp-today/acwa-power-scales-tower-trough-design-set-record-low-csp-price [accessed: 02/07/2018].
[57] Islam Md Tasbirul, Huda Nazmul, Abdullah AB, Saidur R. A comprehensive review of state-of-the-art concentrating solar power (csp) technologies: current status and research trends. Renew Sustain Energy Rev 2018;91:987–1018.
[58] Vignarooban K, Xu Xinhai, Arvay A, Hsu Keng, Kannan AM. Heat transfer fluids for concentrating solar power systems—a review. Appl Energy 2015;146:383–96.